Published in final edited form as:
Cell. 2010 November 12; 143(4): 592–605. doi:10.1016/j.cell.2010.10.032.

Germinal Center Dynamics Revealed by Multiphoton Microscopy Using a Photoactivatable Fluorescent Reporter

Gabriel D. Victora[1,2], **Tanja A. Schwickert**[1], **David R. Fooksman**[2], **Alice O. Kamphorst**[1], **Michael Meyer-Hermann**[3], **Michael L. Dustin**[2,5], and **Michel C. Nussenzweig**[1,4,5,*]

[1] Laboratory of Molecular Immunology, The Rockefeller University, New York, NY 10065, USA

[2] Martin and Helen Kimmel Center for Biology and Medicine, Skirball Institute of Biomolecular Medicine, New York University School of Medicine, New York, NY 10016, USA

[3] Department Systems Immunology, Helmholtz Centre for Infection Research, Inhoffenstr. 7, D-38124, Braunschweig, Germany

[4] Howard Hughes Medical Institute, The Rockefeller University, New York, NY 10065, USA

SUMMARY

The germinal center (GC) reaction produces high-affinity antibodies by random mutation and selective clonal expansion of B cells with high-affinity receptors. However, the mechanism by which B cells are selected remains unclear, as does the role of the two anatomically-defined areas of the GC, light zone (LZ) and dark zone (DZ). We combined a new transgenic photoactivatable green fluorescent protein (PA-GFP) tracer with multiphoton laser-scanning microscopy and flow cytometry to examine anatomically defined LZ and DZ B cells and GC selection. We find that B cell division is restricted to the DZ, and that there is a net vector of B cell movement from the DZ to the LZ. The decision to return from the LZ to the DZ and undergo clonal expansion is controlled by T cells, which discern between LZ B cells based on the amount of antigen captured, providing a mechanism for GC selection.

INTRODUCTION

Germinal centers (GCs) were first described in the 19th century as distinct microanatomical regions in lymphoid organs that contained dividing cells, and were long believed to be the sites of lymphocyte development (Nieuwenhuis and Opstelten, 1984). It has since become evident that, in fact, GCs are the site of antigen-dependent clonal expansion, immunoglobulin diversification, and affinity maturation (Allen et al., 2007a; Klein and Dalla-Favera, 2008; MacLennan, 1994; Rajewsky, 1996; Tarlinton, 2008), all of which are required for the generation of the high-affinity antibodies that make up the core of the humoral immune response.

*Correspondence: nussen@rockefeller.edu.
[5]These authors contributed equally to this work

ACCESSION NUMBERS

The GEO accession number for the microarray data reported in this paper is GSM589872.

Affinity maturation is defined as the gradual increase in the affinity of serum antibodies following infection or immunization (Eisen and Siskind, 1964; Goidl et al., 1968; Nussenzweig and Benacerraf, 1967). This process occurs in the GC as the result of random somatic hypermutation of B cell receptor (BCR) genes (McKean et al., 1984) followed by Darwinian-like selection of B cell clones with increased affinity for antigen (Allen et al., 2007a; Klein and Dalla-Favera, 2008; MacLennan, 1994; Rajewsky, 1996; Tarlinton, 2008). Despite the importance of affinity-based selection, there is little understanding of the mechanisms by which this process is controlled within the GC.

Early histological studies advanced the idea that the GC is divided into two anatomically distinct regions: a dark zone (DZ), containing large, mitotically active B cells known as *centroblasts*; and a light zone (LZ), containing smaller, non-dividing B cells known as *centrocytes*, as well as antigen deposited on the surface of follicular dendritic cells (FDCs) and antigen-specific follicular T helper cells (Allen et al., 2007a; Klein and Dalla-Favera, 2008; MacLennan, 1994; Nieuwenhuis and Opstelten, 1984; Rajewsky, 1996; Tarlinton, 2008). This segregation between cell division and potential selecting agents suggested a model in which selection would require the migration of cells between the two zones, the DZ acting as a source of B cells with mutated BCRs that would then undergo selection in the LZ (MacLennan, 1994), possibly returning to the DZ for further proliferation and mutation (Meyer-Hermann et al., 2001; Oprea and Perelson, 1997).

Recent live imaging studies demonstrated that B cells do indeed move bi-directionally between the two GC zones (Allen et al., 2007b; Hauser et al., 2007a; Schwickert et al., 2007). Although these studies were able to show bi-directional B cell exchange between zones, the length of the imaging window and the number of events documented were insufficient to draw firm conclusions regarding the dynamics of GC selection (Allen et al., 2007a; Figge et al., 2008; Meyer-Hermann et al., 2009). Furthermore, GC B cells in the two zones appeared similar in size and morphology, and showed similar levels of DNA synthesis, challenging the traditional description of small, non-dividing centrocytes and large, cycling centroblasts (Allen et al., 2007b; Hauser et al., 2007a; Schwickert et al., 2007). Finally, studies in which zonal migration was disrupted failed to show alterations in cell division, GC size or development of high affinity anti-NP antibodies (Allen et al., 2004; Nie et al., 2004). Together with the initial short-term imaging studies, these physiologic experiments called into question the importance of polarization of the GC into LZ and DZ in terms of selection.

Another key unresolved issue is precisely how antigen-driven selection is regulated. Traditionally, two non-mutually exclusive possibilities have been considered based on the signals available to B cells in the GC. According to the classical model, B cells with higher-affinity receptors would be selected as a result of BCR crosslinking by antigen deposited on the FDC surface (Tarlinton and Smith, 2000). A second possibility is that GC B cells use their BCRs to capture and internalize antigen deposited in the LZ for presentation to GC-resident T cells. These specialized T helper cells would in turn influence B cell selection through cytokine secretion or co-receptor ligation (Allen et al., 2007a; Tarlinton, 2008; Vinuesa et al., 2005b). Despite the wealth of studies addressing this question, the available evidence is both circumstantial and contradictory, and models of the way in which selection takes place in the GC remain speculative (Allen et al., 2007a; Hauser et al., 2007b; Meyer-Hermann et al., 2006; Tarlinton, 2008).

Solving the issue of how GC selection operates would require a precise definition of the characteristics of LZ and DZ B cells and of the migration patterns of these cell populations *in vivo*. To this end, we developed a method for *in situ* microanatomical labeling and long-term *in vivo* imaging of GC B cells that combines a new transgenic mouse that expresses

photoactivatable green fluorescent protein (PA-GFP) (Patterson and Lippincott-Schwartz, 2002), multiphoton laser scanning microscopy, and flow cytometry. Here, we report on the characteristics of LZ and DZ GC B cells and on the dynamic mechanisms that limit interzonal migration and affinity-based selection during the humoral immune response.

RESULTS

Photoactivation

PA-GFP is a green fluorescent protein variant whose peak excitation wavelength shifts from ~415 nm to ~495 nm upon one-photon irradiation at ~415 nm or two-photon irradiation at ~720–840 nm (Patterson and Lippincott-Schwartz, 2002; Schneider et al., 2005). To examine selection in the GC, we produced transgenic mice in which all hematopoietic cells express PA-GFP (Fig. S1A–C). PA-GFP-expressing cells can be photoactivated within intact lymph nodes with great microanatomical precision (~10 microns in the Z dimension, or close to one cell diameter; Fig. 1A) by two-photon irradiation at 830 nm, and subsequently identified by two-photon excitation at 940 nm (Supplementary Movie S1) or flow cytometry using a conventional 488 nm laser (Fig. 1B). After a brief recovery period, the migration of photoactivated naïve T and GC B cells is indistinguishable from that of control cells (Fig. 1C–D, Supplementary Movie S2, and below). The half-life of photoactivated PA-GFP in naïve B cells was estimated to be 30h (Fig. S1D), a figure consistent with previous estimates for the half-life of GFP in living cells (Corish and Tyler-Smith, 1999; Nagaoka et al., 2000).

Photoactivatable Germinal Centers

Although two populations of GC B cells were originally defined based on size, LZ and DZ B cells were found to be indistinguishable in size or movement pattern by multiphoton microscopy (Allen et al., 2007b; Hauser et al., 2007a; Schwickert et al., 2007), and there are no anatomically validated surface markers for the two cell types. To mark LZ and DZ cells directly *in situ*, we produced photoactivatable antigen-specific GCs. PA-GFP mice were bred to B1-8^{hi} heavy chain knock-in mice (PA-GFP/B1-8^{hi}), which carry a heavy chain that, when combined with an Igλ light chain, produces an antibody that is specific for the hapten 4-hydroxy-3-nitrophenylacetyl (NP) (Shih et al., 2002). To generate photoactivatable germinal centers, we used an adaptation of the classical prime-boost model (Katz et al., 1970; Rajewsky et al., 1969; Schwickert et al., 2007). PA-GFP/B1-8^{hi} B cells were transferred into ovalbumin (OVA)-primed mice, which were subsequently challenged subcutaneously with soluble NP-conjugated OVA to produce NP-specific GCs in skin-draining lymph nodes (Fig. 2A). This protocol is preferable for intravital imaging due to the absence of adjuvant-induced inflammation in the draining lymph-node. The GC light zone was identified by injecting NP conjugated to red fluorescent protein tdTomato (Shaner et al., 2004) (NP-tdTomato), which forms immune complexes that bind to FDCs in NP-immunized mice (Fooksman et al., 2010).

LZ and DZ B cells

To determine the phenotype of LZ and DZ B cells, we photoactivated one or the other zone in explanted lymph nodes (Fig. 2B and Supplementary Movie S3) and analyzed the photoactivated cells by flow cytometry. LZ and DZ cells expressed comparable levels of FAS, GL-7 antigen, CD38, and MHC II (Fig. S2A). Consistent with previous immunohistochemical and functional studies (Allen et al., 2004;Liu et al., 1991), LZ cells expressed higher levels of surface immunoglobulin, slightly higher levels of chemokine receptor CXCR5, and lower levels of CXCR4 than DZ cells (Fig. 2C). Cell cycle analysis by DNA content showed that cells in the G2/M phase of the cell cycle were almost entirely restricted to the DZ, whereas cells in S phase were found in both zones (Fig. 2D). Contrary

to the classical description of centrocytes and centroblasts, LZ and DZ B cells were similar in size and were both larger than follicular B cells (Fig. 2E). An exception to this was a small subpopulation of larger DZ cells (5–10%) that corresponds to cells in the G2/M phase of the cell cycle (Fig. S2B).

To further characterize LZ and DZ B cells, we purified photoactivated cells by cell sorting (Fig. 2A) and performed microarray-based gene expression profiling. Only 144 of approximately 45,000 probes reproducibly differed by more than 2-fold between the two compartments (Fig. 3A–B, Table S1). By contrast, comparison of gene expression by either LZ or DZ cells and naive B cells showed a substantially larger difference, with 2,135 and 2,458 probes differing by 2-fold or more, respectively (Fig. 3A). Systematic Gene Ontology analysis of an expanded subset of genes whose expression differed between LZ and DZ by at least 1.33-fold (see Extended Experimental Procedures) showed that probes upregulated in DZ were dominated by genes involved in mitosis, whereas probes upregulated in LZ were enriched in lymphocyte activation markers, cell surface molecules, and regulators of apoptosis (Fig 3B–C, Table S2). To gain insight into the pathways activated in each zone, we conducted gene set enrichment analysis (GSEA) (Mootha et al., 2003;Subramanian et al., 2005) for transcription factor motifs (Xie et al., 2005). This analysis showed strong evidence of NF-κB activation in the LZ, in addition to the signatures of serum response factor (SRF), signal transducer and activator of transcription 5 (STAT5) and c-Myc engagement (Table S3). Since both BCR crosslinking and T cell signals delivered via CD40 are capable of activating the NF-κB pathway in LZ, we conducted a further GSEA analysis overlaying gene signatures of CD40 and BCR ligation (Basso et al., 2004;Zhu et al., 2004). This analysis showed the LZ population to be strongly imprinted with the signatures of both of these activation signals (Fig. 3D and Table S3). Taken together, our cell cycle and gene expression analyses support the notion that cells in the two zones differ in a functionally significant manner.

To identify markers capable of distinguishing DZ and LZ cells by flow cytometry, we screened photoactivated LZ or DZ B cells on the basis of the gene array results for differentially expressed surface molecules. Two markers, CD86 and CD83, were able to distinguish between LZ and DZ cells by flow cytometry when combined with CXCR4: LZ cells are $CXCR4^{lo}CD86^{hi}CD83^{hi}$ and DZ cells are $CXCR4^{hi}CD86^{lo}CD83^{lo}$ (Fig. 4A and B). To validate the gene array results obtained with $B1\text{-}8^{hi}$ NP-specific B cells we examined polyclonal LZ and DZ GC cells from immunized wild-type mice identified using these markers (Fig. S3A). Flow cytometric analysis (Fig. 4C and S3B) or cell sorting followed by qPCR (Fig. S3C and 4D) confirmed the differential expression in LZ and DZ of all 23 genes tested. Furthermore, LZ and DZ cells in these mice showed the same cell cycle distribution as those identified by photoactivation (Fig. 4E and S3D). Therefore, LZ and DZ B cells in polyclonal GCs from wild-type mice are phenotypically indistinguishable from their $B1\text{-}8^{hi}$ counterparts. We conclude that the combination of photoactivation and flow cytometry allows for unambiguous identification of LZ and DZ GC B cells based on microanatomical location. The LZ contains cells whose gene expression profile is consistent with antigen encounter and T-B cell interaction, whereas cells in the DZ are poised to undergo cell division.

Interzonal migration

To examine the exchange of GC B cells between zones over an extended period of time, we photoactivated NP-specific LZ or DZ cells in popliteal lymph nodes of living mice and tracked their migration at one-hour intervals for up to 6 hours (Fig. 5A–D). Photoactivated cells were monitored for viability throughout these analyses by comparing their motility to that of control CFP^{+} GC cells in the same sample. Photoactivated LZ and DZ cells were

similar to control cells in terms of morphology and speed of movement for up to 8 hours after photoactivation (Fig. 5E and Supplementary Movies S4 and S5).

Following photoactivation, DZ B cells migrated rapidly to the LZ, with up to 50% of cells reaching the opposite zone by 4 hours (Fig. 5B and D). In stark contrast, photoactivated LZ B cells crossed into the DZ at a much lower rate, with less than 15% making the transition over a 6-hour period (Fig. 5C–D). Similar results were obtained when B-Phycoerythrin immune complexes were used to label the LZ instead of NP-tdTomato (Allen et al., 2007b) (Fig. 5D). Thus, there is a strong net flux of cells from DZ to LZ, with only a few cells returning from LZ to DZ. Importantly, measurements made 30 minutes after photoactivation showed only a minor difference in the percentage of cells migrating from DZ to LZ (5.7%, +/− 2.2%) and LZ to DZ (3.7%, +/− 0.7%), potentially accounting for the inability of prior studies to detect a net vector in interzonal migration.

To determine what these rates of migration imply in terms of selection, we modeled the interzonal migration data using an ordinary differential equation model for the dynamics of photoactivated B cells in GC zones (see Extended Experimental Procedures for details). This approach yielded migration rates of 15%/hour for DZ to LZ and 3%/hour for LZ to DZ, which corresponds to a fraction of LZ cells selected to return to DZ of 30% in this experimental system. The fitting of the simulated data to the experiment is shown in Fig. S4. Similar results were obtained using a more complex agent-based model of GC dynamics, morphology and affinity maturation published previously (not shown) (Figge et al., 2008). Combined with the finding that mitosis is restricted to the DZ, the net flow of cells from the DZ to the LZ strongly suggests that selection is driven by competition among LZ cells for signals capable of promoting their return to the DZ for further rounds of proliferation.

Access to T cell help limits interzonal migration and GC selection

To gain insight into which signals may be required for LZ to DZ migration, we initially took advantage of the fact that, in addition to the transferred B1-8^{hi} B cells, GCs in our transfer model (Fig. S5A) also contain a minor population (~10%) of endogenous B cells (Fig. S5B), which likely represents a mixture of OVA- and NP-specific cells. This population displays a skewed DZ/LZ ratio (~0.5:1, as opposed to ~2:1 among B1-8^{hi} cells) and a lower proliferation rate, consistent with of a lower rate of selection (Fig. S5B). To determine whether this is a consequence of the inability of endogenous cells to compete with the B1-8^{hi} population for signals that regulate return to the DZ, we depleted NP-specific cells from the GC by treatment with a large dose of NP-dextran, which strongly crosslinks the BCR of NP-specific cells. Consistent with the observation that BCR crosslinking results in GC B cell apoptosis (Han et al., 1995b;Pulendran et al., 1995;Shokat and Goodnow, 1995), injection of NP-dextran led to a marked loss of B1-8^{hi} cells from the GC (Fig. S5C). This loss was followed by a shift in the DZ/LZ ratio of the endogenous cells to almost B1-8^{hi} levels (DZ/LZ ratio = 1.4:1), along with a robust increase in endogenous B cell proliferation and representation in the GC (Fig. S5C). This data implies that migration of GC cells from LZ to DZ is controlled by competition for access to a limiting factor.

One such limiting factor could be the T helper cells present in the GC LZ, which might regulate selection on the basis of a B cell's ability to present cognate antigen (Allen et al., 2007a; Meyer-Hermann et al., 2006; Tarlinton, 2008). This model has been difficult to evaluate directly due to the lack of a suitable method for delivering T cell help without crosslinking the BCR. To isolate antigen capture from BCR crosslinking, we took advantage of the observation that GC B cells express high levels of DEC205, a cell-surface lectin that delivers antigen to MHC-containing processing compartments (Fig. S5D; (Jiang et al., 1995; Kamphorst et al., 2010). Protein antigens such as OVA can be delivered to DEC205-expressing GC cells independently of BCR by using chimeric antibodies to DEC205

(αDEC-OVA). Targeting B cells in this manner results in efficient processing and presentation of OVA peptides (Fig. S5E; (Kamphorst et al., 2010).

To test the role of antigen presentation in interzonal migration, we produced mixed GCs containing DEC205$^{+/+}$ and DEC205$^{-/-}$ B1-8^{hi} B cells by immunizing wild-type mice that had received a mixture of the two cell types (Fig. 6A). αDEC-OVA treatment initially resulted in a striking accumulation of DEC205$^{+/+}$ cells in the LZ compartment (Fig 6B–C). However, by 24 hours after antigen delivery, DEC205$^{+/+}$ cells began to re-appear in the DZ, and by 48 hours as much as 90% of this population was in the DZ (Fig. 6B–C). Acquisition of DZ phenotype by DEC205$^{+/+}$ cells was accompanied by a burst in proliferation and a consequent increase in the relative number of these cells in the GC (Fig. 6B–D). Histological examination confirmed the relationship between expression of cell-surface markers and zonal localization (Fig. 6E). In contrast, we found no alterations in GC B cell distribution or proliferation in DEC205$^{-/-}$ cells in the same mice (Fig 6B–D). Moreover, targeting with αDEC205 fused to an irrelevant antigen, *Plasmodium falciparum* circumsporozoite protein (αDEC-CS; (Boscardin et al., 2006) had no effect on any GC B cell population (Fig. S5F). Although there is no known cross-reactivity between the NP-specific B1-8^{hi} BCR and OVA, we examined the possibility of synergistic effects of DEC205 and BCR ligation by targeting GC B cells in NP-keyhole limpet hemocyanin (KLH) immunized mice with αDEC-OVA, as well as by co-crosslinking the two receptors with NP-conjugated αDEC205. Neither approach induced LZ to DZ migration or B cell expansion (Fig. S5G), demonstrating that the effect of αDEC-OVA targeting is fully dependent on the specificity of GC T cells. We conclude that targeting T cell help to GC B cells is sufficient to induce *en masse* migration of the targeted population from LZ to DZ, and that T cell help is therefore limiting for interzonal migration.

To determine whether T cell help is also limiting for clonal expansion, we examined mixed GCs containing both DEC205$^{+/+}$ and DEC205$^{-/-}$ B1-8^{hi} B cells 72h after treatment with αDEC-OVA (Fig. 7A). Whereas control GCs targeted with an irrelevant antigen, αDEC-CS, maintained a ratio of DEC205$^{+/+}$ to DEC205$^{-/-}$ similar to the initial transfer (1:4), αDEC-OVA-targeted GCs were composed almost exclusively of DEC205$^{+/+}$ cells (Fig. 7B and Fig S6A. Importantly, the expansion of DEC205$^{+/+}$ cells was accompanied by decrease in the rate of cell division and skewing of the DZ/LZ ratio among the non-targeted (DEC205$^{-/-}$) population (from ~1.7:1 to 0.9:1; Fig. 7C). The finding that the DEC205$^{-/-}$ majority is counterselected by focusing T cell help on a small subset of DEC205$^{+/+}$ cells indicates that T cell help is indeed limiting for clonal expansion. Furthermore, αDEC-OVA treatment also led to a marked increase in the number of DEC205$^{+/+}$ plasmablasts in targeted lymph nodes (Fig. 7D–F), showing that T cell help is also capable of controlling this other cell fate decision.

To determine whether restricting T cell help to high-affinity cells is a requirement for affinity maturation, we measured the effect of DEC205 targeting on the affinity of anti-NP serum antibodies in wild-type NP-OVA-immunized mice (Fig. S6B). Since T cell help in targeted mice would be distributed among all GC cells irrespective of BCR affinity, we would expect such treatment to abrogate affinity maturation. As expected from the increase in plasmablasts in response to αDEC-OVA in the transfer experiments (Fig. 7E–F), we found a significant increase in anti-NP titers in targeted mice (Fig. 7G). However, in contrast to control mice, the antibodies in αDEC-OVA-treated mice failed to undergo affinity maturation, as measured by the ratio of anti-NP_3 to anti-NP_{23} titers (Fig. 7G). Absence of affinity maturation in αDEC-OVA targeted mice was also documented by their relative failure to accumulate the W33L mutation characteristic of high-affinity anti-NP antibodies (Allen et al., 1988), despite comparable overall mutation rates (Fig. S6C, Fig. 7H, and data not shown). Together, these experiments suggest that affinity maturation is abrogated when

GC B cells receive T cell help independently of BCR affinity, and that, under conditions of equal T cell help, differential BCR crosslinking is not sufficient to mediate affinity-based selection. We conclude that T cell help is a limiting factor for B cell selection in GCs.

DISCUSSION

We used a combination of photoactivatable GFP, multiphoton microscopy and flow cytometry to address long-standing questions regarding the mechanisms that govern selection in GCs. The results reveal distinct physiologic functions for the two anatomically defined GC compartments and suggest a cellular mechanism that limits affinity-based selection.

LZ and DZ cells

The morphological and dynamic similarities between cells in the two GC zones revealed by intravital microscopy blurred the classical distinction between centrocytes and centroblasts (Allen et al., 2007b; Hauser et al., 2007a; Schwickert et al., 2007) to the extent that the existence of two distinct populations was called into question (Allen et al., 2007a). Two of the features traditionally thought to distinguish between these two populations were size – centroblasts being larger – and expression of surface immunoglobulin – thought to be higher in centrocytes (MacLennan, 1994). However, the size of B cells in the LZ and the level of surface immunoglobulin expression is virtually impossible to infer by histology (Allen et al., 2007a; Nieuwenhuis and Opstelten, 1984). While highly desirable, clear distinction between the two cell types by flow cytometry was also not possible due to the lack of anatomically validated markers (Allen et al., 2007a; Hogerkorp and Borrebaeck, 2006).

In situ photoactivation combined with flow cytometry resolves these problems by providing direct microanatomical information that allows for the unequivocal identification of LZ and DZ cells. In agreement with the initial multiphoton studies, we find that LZ and DZ cells are virtually equal in size (Allen et al., 2007b; Hauser et al., 2007a; Schwickert et al., 2007). However, despite their similarities, the two cell types differ in a number of important respects. Global gene expression analysis indicates that GCs are highly compartmentalized, with LZ cells showing evidence of ongoing BCR and CD40 signaling activity consistent with antigen-dependent selection. In contrast, DZ cells specialize in cell division, and express higher levels of Polη, which mediates error prone repair during somatic hypermutation (Delbos et al., 2005). Our data appear to refute recent claims that cell division occurs in both the LZ and the DZ (Allen et al., 2007b; Hauser et al., 2007a). However, the methods used in those studies labeled cells in the S phase of the cell cycle, and the results are therefore not incompatible with the idea that GC cells enter into S phase in the LZ, possibly in response to activation signals present in that zone, but leave this compartment before progressing to mitosis.

Interzonal migration among GC B cells

Multiphoton live imaging studies provided the first concrete evidence for bidirectional GC B cell movement between zones (Allen et al., 2007b; Hauser et al., 2007a; Schwickert et al., 2007). However, due to limitations inherent to multiphoton microscopy (Allen et al., 2007a; Germain et al., 2006), the number of events was too small for robust statistical analysis (Figge et al., 2008). Moreover, true interzonal migrants could not always be distinguished from cells temporarily crossing the DZ/LZ border or exiting the GC from one zone while passing through the other. The combination of multiphoton imaging with PA-GFP allowed us to overcome these limitations by circumventing the need to track individual GC cells and enabled observation of the entire GC for periods of several hours. These longer-term experiments revealed polarized net movement of B cells from DZ to LZ, consistent with the

idea that movement between zones supports iterative cycles of selection (Meyer-Hermann et al., 2001; Oprea and Perelson, 1997).

Mathematical modeling of our data using a simplified phenomenological model showed that roughly 30% of cells in the LZ are selected to return to the DZ. Though this model agrees with the experimental data to within one standard deviation, we expect that a more detailed model is needed to describe the complex process of interzonal migration. Particularly, it seems that saturation of the DZ to LZ migration frequency occurs faster in experiment than in theory. While the reason for this is unclear, one possibility is that the DZ may comprise a heterogeneous population of cells with different migration properties (e.g., pre- and post-mitotic cells), or that a proportion of DZ cells may be arrested in this zone due to genetic errors generated by somatic hypermutation.

Interaction with T cells is limiting for affinity-based selection

Selection of high-affinity B cells in GCs is believed to be mediated by limiting amounts of antigen on the surface of FDCs (Eisen and Siskind, 1964; Goidl et al., 1968; Nussenzweig and Benacerraf, 1967). It has been proposed that this effect is governed by direct signals derived from BCR crosslinking (Brink et al., 2007; Liu et al., 1989; Manser, 2004; Paus et al., 2006; Phan et al., 2006; Tarlinton and Smith, 2000). However, in addition to signaling, the BCR is also an endocytic receptor that captures antigen for processing and presentation to T cells (Lanzavecchia, 1985; Rock et al., 1984). Thus, an alternative, though non-exclusive, model for selection in the GC is that it is mediated by helper T cells, which recognize peptide-MHC presented on the surface of high affinity B cells (Allen et al., 2007a; Meyer-Hermann et al., 2006; Tarlinton, 2008; Vinuesa et al., 2005b). The role of the BCR in this model would be to retrieve antigen from the FDC surface, with affinity dictating the relative amount of antigen captured (Batista et al., 2001; Suzuki et al., 2009).

While it is clear that both BCR and T cell-delivered signals are necessary for GC maintenance (Han et al., 1995a; Huntington et al., 2006), and that each of these signals is capable of extending B cell survival *in vitro* (Liu et al., 1989), evidence for one or the other or both as agents of selection in the GC is circumstantial (Allen et al., 2007a; Tarlinton, 2008). Importantly, no experimental models to date have been able to acutely induce the selection of a specific GC population *in vivo*. Our experiments show that helper T cells can control interzonal migration by directing B cells that capture antigen to return from the LZ to the DZ, where they undergo clonal expansion. Similarly, helper T cells also appear to regulate a B cell's decision to develop into an antibody-secreting plasmablast (Fig. 7F–G). The finding that targeting T cell help to GC B cells leads to their selective expansion and differentiation at the expense of non-targeted cells implies that T cell help is limiting for GC selection. This notion is supported by previous work showing that deregulated T cell help in *Sanroque* mutant mice leads to faulty GC selection and to the emergence of autoantibody-producing B cells (Vinuesa et al., 2005a). While our experiments do not rule out a role for BCR crosslinking in selection, they suggest that antigen receptor crosslinking is neither limiting nor sufficient for selection when B cells with receptors of different affinities display equivalent levels of peptide-MHC (Fig 7G–H). Under physiological conditions, it is likely that both BCR-based signaling and T cell help, in addition to signals from FDCs and via TLRs, are likely to interact to facilitate affinity maturation.

A dynamic model of GC selection

The exquisite dependence of T cell-induced selection on migration between zones shown in our experiments suggests a highly polarized GC structure, with different compartments specialized in selection and proliferation. We propose a model wherein signals from antigen in the LZ initially entrap specific B cells in this zone. Subsequent presentation of peptide-

MHC to follicular helper T cells produces signals that eventually lead to B cell migration to the DZ. Although both high- and low-affinity B cells can capture antigen, the amount of antigen captured will be directly proportional to the affinity of their BCRs, leading to an affinity-dependent difference in the amount of processing and presentation. A limiting number of T cells then selects those B cells with the highest peptide-MHC density (Depoil et al., 2005) and directs their return to the DZ, where they undergo rapid division. Conversely, LZ cells that fail to be selected are relatively enriched in the LZ, where they eventually undergo apoptosis – as suggested by the enhanced expression of pro-apoptotic genes in this compartment. Although affinity maturation in this model does not require the active selection of high-affinity clones into the plasma cell fate, this process seems also to be regulated by the same mechanism. We conclude that T helper cells limit the selection of GC B cells by triggering their return from the LZ to the DZ in a functionally compartmentalized GC.

While transgenic mice expressing photoconvertible fluorescent proteins have been reported previously (Nowotschin and Hadjantonakis, 2009; Tomura et al., 2008), this is the first time, to our knowledge, that transgenic PA-GFP has been combined with multiphoton microscopy and flow cytometry to allow precise labeling, tracking and molecular analysis of cells deep within living tissues. This powerful combination of tools is likely to be applicable to problems in other areas of biology.

EXPERIMENTAL PROCEDURES

Mice

PA-GFP-transgenic mice were generated by cloning the PA-GFP ORF (Patterson and Lippincott-Schwartz, 2002) downstream of the human Ubiquitin C promoter (Schaefer et al., 2001). A linearized 2.7 Kb fragment containing the transgene was injected into C57BL/6 (B6) fertilized female pronuclei. Wild-type B6, B6.SJL, and B10.BR mice, as well as B6 mice ubiquitously expressing ECFP, dsRed, or EGFP, were purchased from Jackson Laboratories. B1-8^{hi} knock-in (Shih et al., 2002) and DEC205$^{-/-}$ mice (Guo et al., 2000) were generated and maintained in our laboratory.

Photoactivation and *in vivo* imaging

Cells were photoactivated by scanning with a femtosecond-pulsed multiphoton laser tuned to 830 nm wavelength, and then imaged at 940 nm wavelength. Conditions for photoactivation and intravital imaging are detailed in the Extended Experimental Procedures.

Image analysis

Cell position in interzonal migration time courses was scored manually in 3D using Imaris software v. 6.4.0, as detailed in the Extended Experimental Procedures. Cells were only considered as being in the zone opposite to that of photoactivation after having crossed a transitional area of weak FDC staining.

In situ labeling for flow cytometry and cell sorting

Carefully dissected lymph nodes were placed between two microscope coverslips, held apart using vacuum grease. For each individual lymph node, either DZ or LZ was photoactivated. When possible, LZ and DZ were photoactivated in contralateral nodes from the same mouse. Individual nodes were processed immediately after photoactivation, and pools of 3–5 nodes per condition were stained for flow cytometry with the reaagents listed in Table S4. For microarray experiments, samples were kept on ice or at 4°C during all stages from dissection to sorting.

Microarray

Photoactivated LZ or DZ germinal center cells were sorted directly into Trizol® reagent (Invitrogen). RNA from pooled samples from 15–20 lymph nodes containing at least 1.2×10^4 cells was subjected to 2-round amplification using the Affymetrix 3′ IVT Express Kit. cDNA was hybridized to GeneChip MOE430 2.0 arrays (Affymetrix) according to the manufacturer's instructions. RNA extraction, amplification and hybridization were carried out at the Memorial Sloan Kettering Cancer Center (MSKCC) Genomics Facility.

qPCR

LZ and DZ cells were sorted directly into Trizol LS® reagent (Invitrogen) and RNA extraction was carried out according to the instructions provided by the manufacturer. RNA was reverse-transcribed using random hexamers and SuperscriptII® reverse transcriptase (Invitrogen). Reverse-transcribed RNA was amplified using the primers presented in Table S5 and SYBR Green PCR mix (Applied Biosciences). All primers were designed to span at least one intron. Expression levels were normalized to *Gapdh* and fold changes were calculated by dividing normalized expression in LZ by DZ.

Anti-DEC205 treatment

αDEC-OVA, αDEC-CS, αDEC-$HEL_{48–62}$, and ISO-$HEL_{48–62}$ were produced as chimeric antibodies in 293T cells as described (Boscardin et al., 2006), and injected into mice with ongoing germinal centers as detailed for each experiment.

Statistical analysis

Comparisons between different populations within the same sample or between pairs of samples from the same experiment were done by paired T test. Other pair comparisons were done by Mann-Whitney U test. Comparisons between three groups were done by Kruskall-Wallis test with Dunn's multiple comparison post-test. The proportion of high-affinity sequences in αDEC-OVA and αDEC-CS-treated mice was compared by χ^2 test with Yates correction. All analyses were carried out using Prism software v. 5.0 (Graphpad).

Supplementary Material

Refer to Web version on PubMed Central for supplementary material.

Acknowledgments

We would like to thank J. Lippincott-Schwartz (NIH), R. Tsien (UCSD), and B. Schaefer (USU) for the PA-GFP, tdTomato, and UbC constructs, respectively; the MSKCC Genomics Facility for performing the microarray experiments; J. Zavadil (NYU) for guidance in microarray analysis; A. North and S. Bhuvanendran (Rockefeller University Bio-Imaging Resource Center) for help with multiphoton imaging; R. Scheuerman (University of Texas Southwestern Medical Center) for ACS gene lists for GSEA analysis; and T. Cameron for helpful discussion. This work was supported in part by NIH grants R01 AI072529 (MCN and MLD) and P01 AI071195 (MLD). Support for the Rockefeller University multiphoton microscope and cell sorter was granted by the Empire State Stem Cell Fund through NYSDOH Contract #C023046. DRF was supported by NIH training grant CA009161-34. MMH was supported by the EU-NEST project MAMOCELL in FP6. MCN is an HHMI Investigator.

References

Allen CD, Ansel KM, Low C, Lesley R, Tamamura H, Fujii N, Cyster JG. Germinal center dark and light zone organization is mediated by CXCR4 and CXCR5. Nat Immunol 2004;5:943–952. [PubMed: 15300245]

Allen CD, Okada T, Cyster JG. Germinal-center organization and cellular dynamics. Immunity 2007a; 27:190–202. [PubMed: 17723214]

Allen CD, Okada T, Tang HL, Cyster JG. Imaging of germinal center selection events during affinity maturation. Science 2007b;315:528–531. [PubMed: 17185562]

Allen D, Simon T, Sablitzky F, Rajewsky K, Cumano A. Antibody engineering for the analysis of affinity maturation of an anti-hapten response. EMBO J 1988;7:1995–2001. [PubMed: 3138111]

Basso K, Klein U, Niu H, Stolovitzky GA, Tu Y, Califano A, Cattoretti G, Dalla-Favera R. Tracking CD40 signaling during germinal center development. Blood 2004;104:4088–4096. [PubMed: 15331443]

Batista FD, Iber D, Neuberger MS. B cells acquire antigen from target cells after synapse formation. Nature 2001;411:489–494. [PubMed: 11373683]

Boscardin SB, Hafalla JC, Masilamani RF, Kamphorst AO, Zebroski HA, Rai U, Morrot A, Zavala F, Steinman RM, Nussenzweig RS, et al. Antigen targeting to dendritic cells elicits long-lived T cell help for antibody responses. J Exp Med 2006;203:599–606. [PubMed: 16505139]

Brink R, Phan TG, Paus D, Chan TD. Visualizing the effects of antigen affinity on T-dependent B-cell differentiation. Immunol Cell Biol. 2007

Corish P, Tyler-Smith C. Attenuation of green fluorescent protein half-life in mammalian cells. Protein Eng 1999;12:1035–1040. [PubMed: 10611396]

Delbos F, De Smet A, Faili A, Aoufouchi S, Weill JC, Reynaud CA. Contribution of DNA polymerase eta to immunoglobulin gene hypermutation in the mouse. J Exp Med 2005;201:1191–1196. [PubMed: 15824086]

Depoil D, Zaru R, Guiraud M, Chauveau A, Harriague J, Bismuth G, Utzny C, Muller S, Valitutti S. Immunological synapses are versatile structures enabling selective T cell polarization. Immunity 2005;22:185–194. [PubMed: 15723807]

Eisen HN, Siskind GW. Variations in Affinities of Antibodies During the Immune Response. Biochemistry 1964;3:996–1008. [PubMed: 14214095]

Figge MT, Garin A, Gunzer M, Kosco-Vilbois M, Toellner KM, Meyer-Hermann M. Deriving a germinal center lymphocyte migration model from two-photon data. J Exp Med 2008;205:3019–3029. [PubMed: 19047437]

Fooksman DR, Schwickert TA, Victora GD, Dustin ML, Nussenzweig MC, Skokos D. Development and migration of plasma cells in the mouse lymph node. Immunity 2010;33:118–127. [PubMed: 20619695]

Germain RN, Miller MJ, Dustin ML, Nussenzweig MC. Dynamic imaging of the immune system: progress, pitfalls and promise. Nat Rev Immunol 2006;6:497–507. [PubMed: 16799470]

Goidl EA, Paul WE, Siskind GW, Benacerraf B. The effect of antigen dose and time after immunization on the amount and affinity of anti-hapten antibody. J Immunol 1968;100:371–375. [PubMed: 4867490]

Guo M, Gong S, Maric S, Misulovin Z, Pack M, Mahnke K, Nussenzweig MC, Steinman RM. A monoclonal antibody to the DEC-205 endocytosis receptor on human dendritic cells. Hum Immunol 2000;61:729–738. [PubMed: 10980384]

Han S, Hathcock K, Zheng B, Kepler TB, Hodes R, Kelsoe G. Cellular interaction in germinal centers. Roles of CD40 ligand and B7-2 in established germinal centers. J Immunol 1995a;155:556–567. [PubMed: 7541819]

Han S, Zheng B, Dal Porto J, Kelsoe G. In situ studies of the primary immune response to (4-hydroxy-3-nitrophenyl)acetyl. IV. Affinity-dependent, antigen-driven B cell apoptosis in germinal centers as a mechanism for maintaining self-tolerance. J Exp Med 1995b;182:1635–1644. [PubMed: 7500008]

Hauser AE, Junt T, Mempel TR, Sneddon MW, Kleinstein SH, Henrickson SE, von Andrian UH, Shlomchik MJ, Haberman AM. Definition of germinal-center B cell migration in vivo reveals predominant intrazonal circulation patterns. Immunity 2007a;26:655–667. [PubMed: 17509908]

Hauser AE, Shlomchik MJ, Haberman AM. In vivo imaging studies shed light on germinal-centre development. Nat Rev Immunol 2007b;7:499–504. [PubMed: 17589541]

Hogerkorp CM, Borrebaeck CA. The human CD77− B cell population represents a heterogeneous subset of cells comprising centroblasts, centrocytes, and plasmablasts, prompting phenotypical revision. J Immunol 2006;177:4341–4349. [PubMed: 16982868]

Huntington ND, Xu Y, Puthalakath H, Light A, Willis SN, Strasser A, Tarlinton DM. CD45 links the B cell receptor with cell survival and is required for the persistence of germinal centers. Nat Immunol 2006;7:190–198. [PubMed: 16378097]

Jiang W, Swiggard WJ, Heufler C, Peng M, Mirza A, Steinman RM, Nussenzweig MC. The receptor DEC-205 expressed by dendritic cells and thymic epithelial cells is involved in antigen processing. Nature 1995;375:151–155. [PubMed: 7753172]

Kamphorst AO, Guermonprez P, Dudziak D, Nussenzweig MC. Route of antigen uptake differentially impacts presentation by dendritic cells and activated monocytes. J Immunol 2010;185:3426–3435. [PubMed: 20729332]

Katz DH, Paul WE, Goidl EA, Benacerraf B. Carrier function in anti-hapten immune responses. I. Enhancement of primary and secondary anti-hapten antibody responses by carrier preimmunization. J Exp Med 1970;132:261–282. [PubMed: 4101344]

Klein U, Dalla-Favera R. Germinal centres: role in B-cell physiology and malignancy. Nat Rev Immunol 2008;8:22–33. [PubMed: 18097447]

Lanzavecchia A. Antigen-specific interaction between T and B cells. Nature 1985;314:537–539. [PubMed: 3157869]

Liu YJ, Joshua DE, Williams GT, Smith CA, Gordon J, MacLennan IC. Mechanism of antigen-driven selection in germinal centres. Nature 1989;342:929–931. [PubMed: 2594086]

Liu YJ, Zhang J, Lane PJ, Chan EY, MacLennan IC. Sites of specific B cell activation in primary and secondary responses to T cell-dependent and T cell-independent antigens. Eur J Immunol 1991;21:2951–2962. [PubMed: 1748148]

MacLennan IC. Germinal centers. Annu Rev Immunol 1994;12:117–139. [PubMed: 8011279]

Manser T. Textbook germinal centers? J Immunol 2004;172:3369–3375. [PubMed: 15004133]

McKean D, Huppi K, Bell M, Staudt L, Gerhard W, Weigert M. Generation of antibody diversity in the immune response of BALB/c mice to influenza virus hemagglutinin. Proc Natl Acad Sci U S A 1984;81:3180–3184. [PubMed: 6203114]

Meyer-Hermann M, Deutsch A, Or-Guil M. Recycling probability and dynamical properties of germinal center reactions. J Theor Biol 2001;210:265–285. [PubMed: 11397129]

Meyer-Hermann M, Figge MT, Toellner KM. Germinal centres seen through the mathematical eye: B-cell models on the catwalk. Trends Immunol 2009;30:157–164. [PubMed: 19282244]

Meyer-Hermann ME, Maini PK, Iber D. An analysis of B cell selection mechanisms in germinal centers. Math Med Biol 2006;23:255–277. [PubMed: 16707510]

Mootha VK, Lindgren CM, Eriksson KF, Subramanian A, Sihag S, Lehar J, Puigserver P, Carlsson E, Ridderstrale M, Laurila E, et al. PGC-1alpha-responsive genes involved in oxidative phosphorylation are coordinately downregulated in human diabetes. Nat Genet 2003;34:267–273. [PubMed: 12808457]

Nagaoka H, Gonzalez-Aseguinolaza G, Tsuji M, Nussenzweig MC. Immunization and infection change the number of recombination activating gene (RAG)-expressing B cells in the periphery by altering immature lymphocyte production. J Exp Med 2000;191:2113–2120. [PubMed: 10859336]

Nie Y, Waite J, Brewer F, Sunshine MJ, Littman DR, Zou YR. The role of CXCR4 in maintaining peripheral B cell compartments and humoral immunity. J Exp Med 2004;200:1145–1156. [PubMed: 15520246]

Nieuwenhuis P, Opstelten D. Functional anatomy of germinal centers. Am J Anat 1984;170:421–435. [PubMed: 6383007]

Nowotschin S, Hadjantonakis AK. Use of KikGR a photoconvertible green-to-red fluorescent protein for cell labeling and lineage analysis in ES cells and mouse embryos. BMC Dev Biol 2009;9:49. [PubMed: 19740427]

Nussenzweig V, Benacerraf B. Antihapten antibody specificity and L chain type. J Exp Med 1967;126:727–743. [PubMed: 4168100]

Oprea M, Perelson AS. Somatic mutation leads to efficient affinity maturation when centrocytes recycle back to centroblasts. J Immunol 1997;158:5155–5162. [PubMed: 9164931]

Patterson GH, Lippincott-Schwartz J. A photoactivatable GFP for selective photolabeling of proteins and cells. Science 2002;297:1873–1877. [PubMed: 12228718]

Paus D, Phan TG, Chan TD, Gardam S, Basten A, Brink R. Antigen recognition strength regulates the choice between extrafollicular plasma cell and germinal center B cell differentiation. J Exp Med 2006;203:1081–1091. [PubMed: 16606676]

Phan TG, Paus D, Chan TD, Turner ML, Nutt SL, Basten A, Brink R. High affinity germinal center B cells are actively selected into the plasma cell compartment. J Exp Med 2006;203:2419–2424. [PubMed: 17030950]

Pulendran B, Kannourakis G, Nouri S, Smith KG, Nossal GJ. Soluble antigen can cause enhanced apoptosis of germinal-centre B cells. Nature 1995;375:331–334. [PubMed: 7753199]

Rajewsky K. Clonal selection and learning in the antibody system. Nature 1996;381:751–758. [PubMed: 8657279]

Rajewsky K, Schirrmacher V, Nase S, Jerne NK. The requirement of more than one antigenic determinant for immunogenicity. J Exp Med 1969;129:1131–1143. [PubMed: 4181830]

Rock KL, Benacerraf B, Abbas AK. Antigen presentation by hapten-specific B lymphocytes. I. Role of surface immunoglobulin receptors. J Exp Med 1984;160:1102–1113. [PubMed: 6207262]

Schaefer BC, Schaefer ML, Kappler JW, Marrack P, Kedl RM. Observation of antigen-dependent CD8+ T-cell/dendritic cell interactions in vivo. Cell Immunol 2001;214:110–122. [PubMed: 12088410]

Schneider M, Barozzi S, Testa I, Faretta M, Diaspro A. Two-photon activation and excitation properties of PA-GFP in the 720–920-nm region. Biophys J 2005;89:1346–1352. [PubMed: 15908572]

Schwickert TA, Lindquist RL, Shakhar G, Livshits G, Skokos D, Kosco-Vilbois MH, Dustin ML, Nussenzweig MC. In vivo imaging of germinal centres reveals a dynamic open structure. Nature 2007;446:83–87. [PubMed: 17268470]

Shaner NC, Campbell RE, Steinbach PA, Giepmans BN, Palmer AE, Tsien RY. Improved monomeric red, orange and yellow fluorescent proteins derived from Discosoma sp. red fluorescent protein. Nat Biotechnol 2004;22:1567–1572. [PubMed: 15558047]

Shih TA, Roederer M, Nussenzweig MC. Role of antigen receptor affinity in T cell-independent antibody responses in vivo. Nat Immunol 2002;3:399–406. [PubMed: 11896394]

Shokat KM, Goodnow CC. Antigen-induced B-cell death and elimination during germinal-centre immune responses. Nature 1995;375:334–338. [PubMed: 7753200]

Subramanian A, Tamayo P, Mootha VK, Mukherjee S, Ebert BL, Gillette MA, Paulovich A, Pomeroy SL, Golub TR, Lander ES, et al. Gene set enrichment analysis: a knowledge-based approach for interpreting genome-wide expression profiles. Proc Natl Acad Sci U S A 2005;102:15545–15550. [PubMed: 16199517]

Suzuki K, Grigorova I, Phan TG, Kelly LM, Cyster JG. Visualizing B cell capture of cognate antigen from follicular dendritic cells. J Exp Med 2009;206:1485–1493. [PubMed: 19506051]

Tarlinton DM. Evolution in miniature: selection, survival and distribution of antigen reactive cells in the germinal centre. Immunol Cell Biol 2008;86:133–138. [PubMed: 18180800]

Tarlinton DM, Smith KG. Dissecting affinity maturation: a model explaining selection of antibody-forming cells and memory B cells in the germinal centre. Immunol Today 2000;21:436–441. [PubMed: 10953095]

Tomura M, Yoshida N, Tanaka J, Karasawa S, Miwa Y, Miyawaki A, Kanagawa O. Monitoring cellular movement in vivo with photoconvertible fluorescence protein “Kaede” transgenic mice. Proc Natl Acad Sci U S A 2008;105:10871–10876. [PubMed: 18663225]

Vinuesa CG, Cook MC, Angelucci C, Athanasopoulos V, Rui L, Hill KM, Yu D, Domaschenz H, Whittle B, Lambe T, et al. A RING-type ubiquitin ligase family member required to repress follicular helper T cells and autoimmunity. Nature 2005a;435:452–458. [PubMed: 15917799]

Vinuesa CG, Tangye SG, Moser B, Mackay CR. Follicular B helper T cells in antibody responses and autoimmunity. Nat Rev Immunol 2005b;5:853–865. [PubMed: 16261173]

Xie X, Lu J, Kulbokas EJ, Golub TR, Mootha V, Lindblad-Toh K, Lander ES, Kellis M. Systematic discovery of regulatory motifs in human promoters and 3′ UTRs by comparison of several mammals. Nature 2005;434:338–345. [PubMed: 15735639]

Zhu X, Hart R, Chang MS, Kim JW, Lee SY, Cao YA, Mock D, Ke E, Saunders B, Alexander A, et al. Analysis of the major patterns of B cell gene expression changes in response to short-term stimulation with 33 single ligands. J Immunol 2004;173:7141–7149. [PubMed: 15585835]

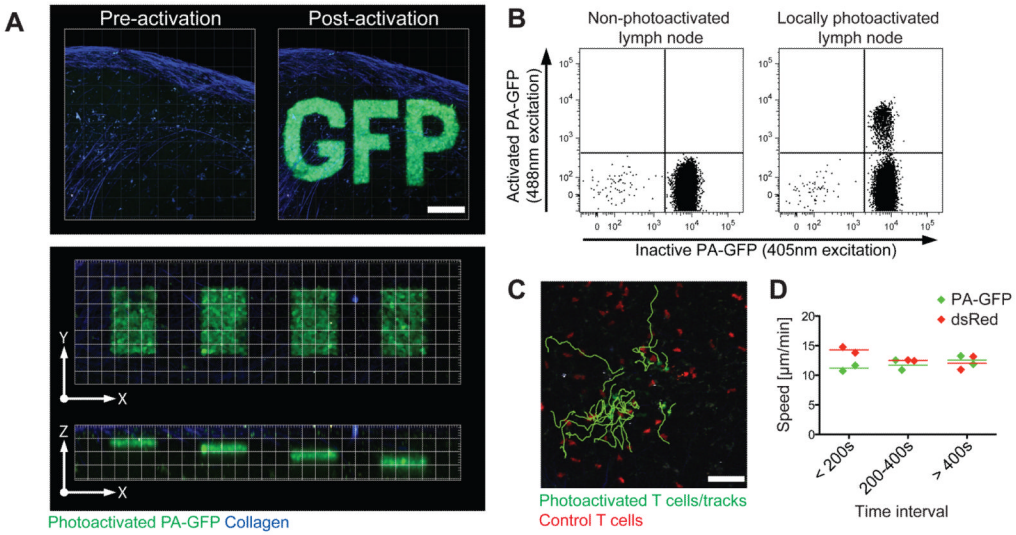

Figure 1. Microanatomical labeling of PA-GFP transgenic B cells

(A) Spatial precision of multiphoton photoactivation of explanted inguinal lymph nodes from PA-GFP transgenic mice. Top: precision in the X–Y-axis. Collapsed Z-stacks (60 μm, 5 μm steps). Scale bar = 100 μm. Imaged at λ=940 nm before and after photoactivation at λ=830 nm of a defined region of interest ("GFP"). Bottom: precision in the Z-axis. X–Y and X–Z views of single planes photoactivated at different Z positions 10 μm apart, from 30 to 60 μm below the LN capsule. Grid = 20 × 20 μm.

(B) Detection of photoactivated cells by flow cytometry. Non-photoactivated (left) and locally photoactivated inguinal lymph nodes from a PA-GFP transgenic mouse were processed in parallel and analyzed for fluorescence under 407 nm (inactive PA-GFP) and 488 nm (activated PA-GFP) excitation (emission filter = 530/30 nm for both). Photoactivation as described for (A).

(C–D) Cells photoactivated *in vivo* remain viable. Tracks (C) of transferred T cells photoactivated *in vivo*. (D) Mean velocity of photoactivated and control cells at different time intervals after photoactivation. All photoactivated cells plus an equal number of randomly selected control cells (dsRed transgenic) outside the photoactivation area were tracked. Each symbol represents one independent experiment (1 movie per experiment, ~20 cells of each type per movie.).

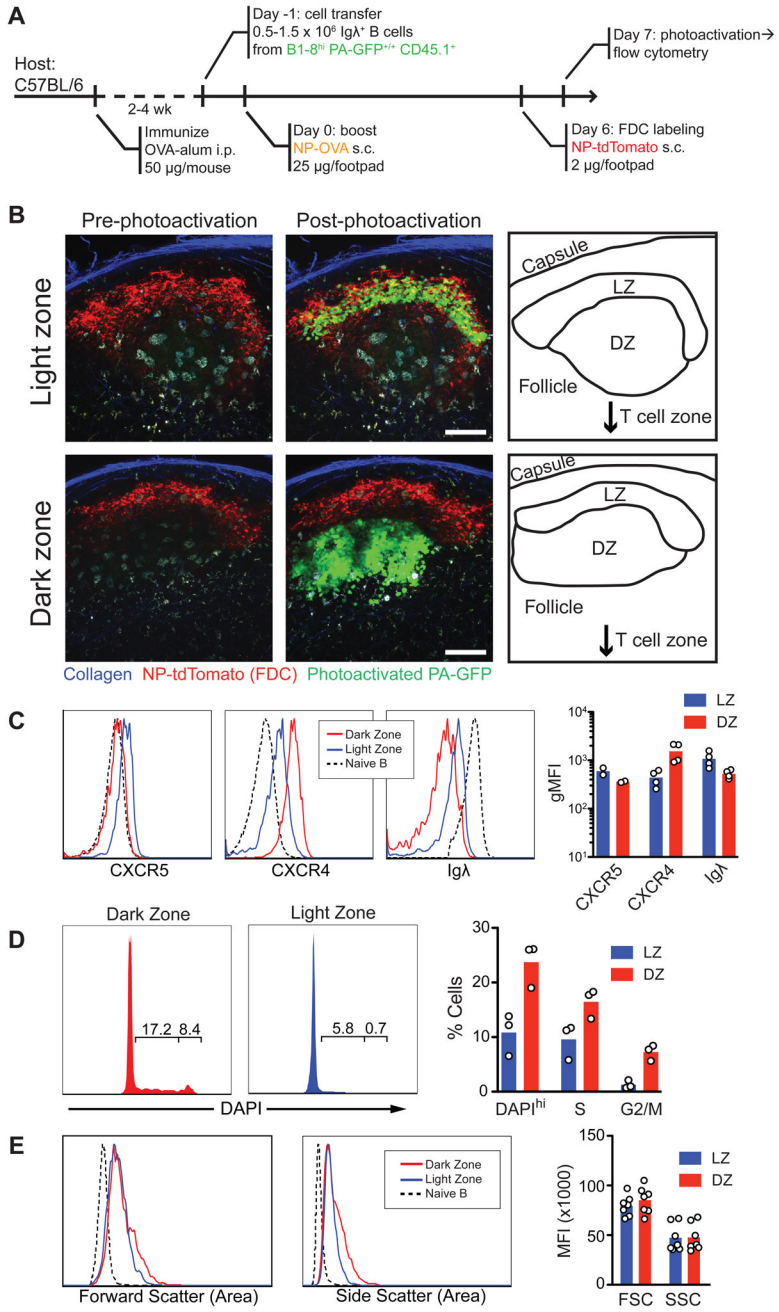

Figure 2. Phenotype of LZ and DZ cells

(A) Diagrammatic representation of the experimental protocol.

(B) Examples of LZ (top row) and DZ (bottom row) multiphoton photoactivation. Collapsed Z-stacks (40 μm, 5 μm steps). Scale bar = 50 μm. Imaged at λ=940 nm before and after photoactivation at λ=830 nm.

(C–E) Chemokine receptor and BCR expression, DNA content (DAPI), and forward and side scatter in photoactivated LZ or DZ cells. GC cells gated as live/single, CD45.1^{+}, FAS^{hi}. Non-GC cells (shown for comparison) gated as Igλ^{+}FAS^{-} Left panels: quantification of flow cytometry data. Each symbol represents one experiment (pools of 3–5 mice per experiment).

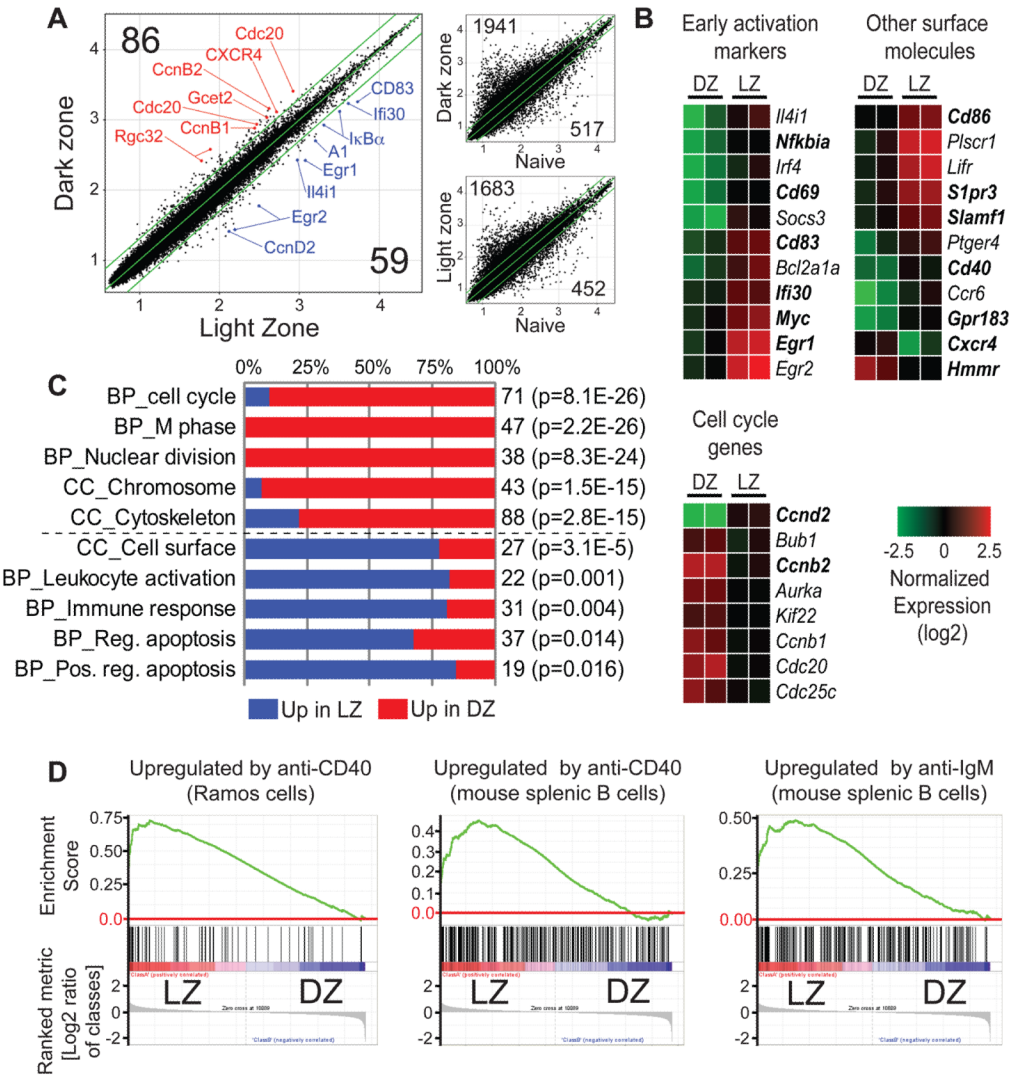

Figure 3. Gene expression in LZ and DZ cells

(A) Differences in gene expression between cells photoactivated in LZ and DZ. Samples generated as indicated in Fig. 2A and sorted as live/single, CD45.1^{+}, FAS^{hi}/GL-7^{+}, activated PAGFP^{+}. Large panel, scatter plots showing raw expression levels (log10) for ~45,000 microarray probes in LZ and DZ. Selected genes are indicated in red (up in DZ) or blue (up in LZ). Smaller panels, differences in gene expression between LZ or DZ and naive B cells, shown for comparison. Green lines indicate 2-fold boundary. Numbers in black indicate the number of genes upregulated by more than 2-fold in the corresponding zone in both replicate assays.

(B) Heatmaps showing normalized expression (log2) of selected genes whose expression differed by more than 2-fold between LZ and DZ in both replicate assays. The full list of genes in this category can be found in Table S1. Genes in bold type were confirmed by either flow cytometry or qPCR.

(C) Gene Ontology (GO) analysis (biological process [BP] and cellular compartment [CC]) of an expanded list of genes differing by at least 1.33-fold between LZ and DZ (see Extended Experimental Procedures and Table S1). Blue and red bars represent the fraction of genes in a given GO category upregulated in LZ and DZ respectively. The total number of genes is indicated to the right of the bar, as is the p-value (Benjamini correction) for

enrichment in the zone with the larger fraction of the genes over the whole mouse genome. An expanded GO analysis is presented in Table S2.

(D) GSEA analysis showing enrichment of gene signatures of CD40 and BCR ligation (gene sets obtained from the literature) in LZ cells. All nominal p-values and FDR rates < 0.001. An expanded GSEA analysis is presented in Table S3.

All data are the average of two experiments, each corresponding to a pool of 15–20 lymph nodes per condition.

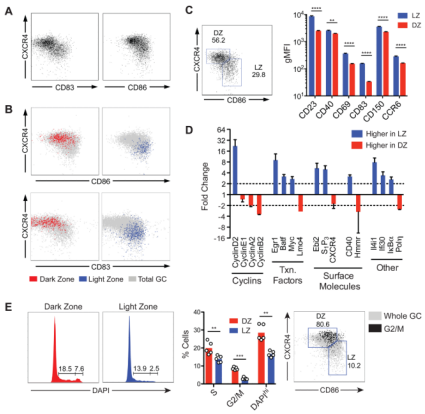

Figure 4. Distinguishing LZ and DZ cells by flow cytometry

(A) Examples of distribution of GC cells according to expression of CXCR4 and CD83 or CD86 in day 7 secondary GCs generated as shown in Fig. 2A. Gated on $B220^{+}CD45.1^{+}CD38^{-}FAS^{+}$.

(B) Distribution of GC cells photoactivated in LZ or DZ according to expression of CXCR4 and CD86 or CD83. Gated on $CD45.1^{+}$, FAS^{hi}, photoactivated $PA\text{-}GFP^{+}$.

(C) Expression of surface markers in LZ and DZ gates by flow cytometry. Polyclonal GCs were generated in wild-type B6 mice as indicated in Fig. S3A, and LZ and DZ populations were defined by expression of CD86 and CXCR4, as shown in the left panel. Right panel, expression of surface markers in LZ and DZ gates. Histograms are presented in Fig. S3B. Representative of 2–3 independent experiments with 2–3 mice each. Error bars represent SEM.

(D) Confirmation of microarray results by qPCR. LZ and DZ cells sorted according to expression of CD86 and CXCR4. GCs generated as in Fig. S3A. Sorting strategy and post-sort purity are shown in Fig. S3C. Graph represents data from two experiments with pools of 10 mice each. Error bars represent SEM.

(E) Cell cycle analysis by DNA content of LZ and DZ cells gated according to expression of CD86 and CXCR4. Left panel, DAPI profiles of cells in LZ and DZ gates. Middle panel, quantification of data from two independent experiments; each symbol represents one mouse. Right panel, cells in G2/M concentrate in the DZ gate. Percentages refer to G2/M cells.

** $p < 0.01$; *** $p < 0.001$; **** $p < 0.0001$, paired T test. Bars = standard error of mean.

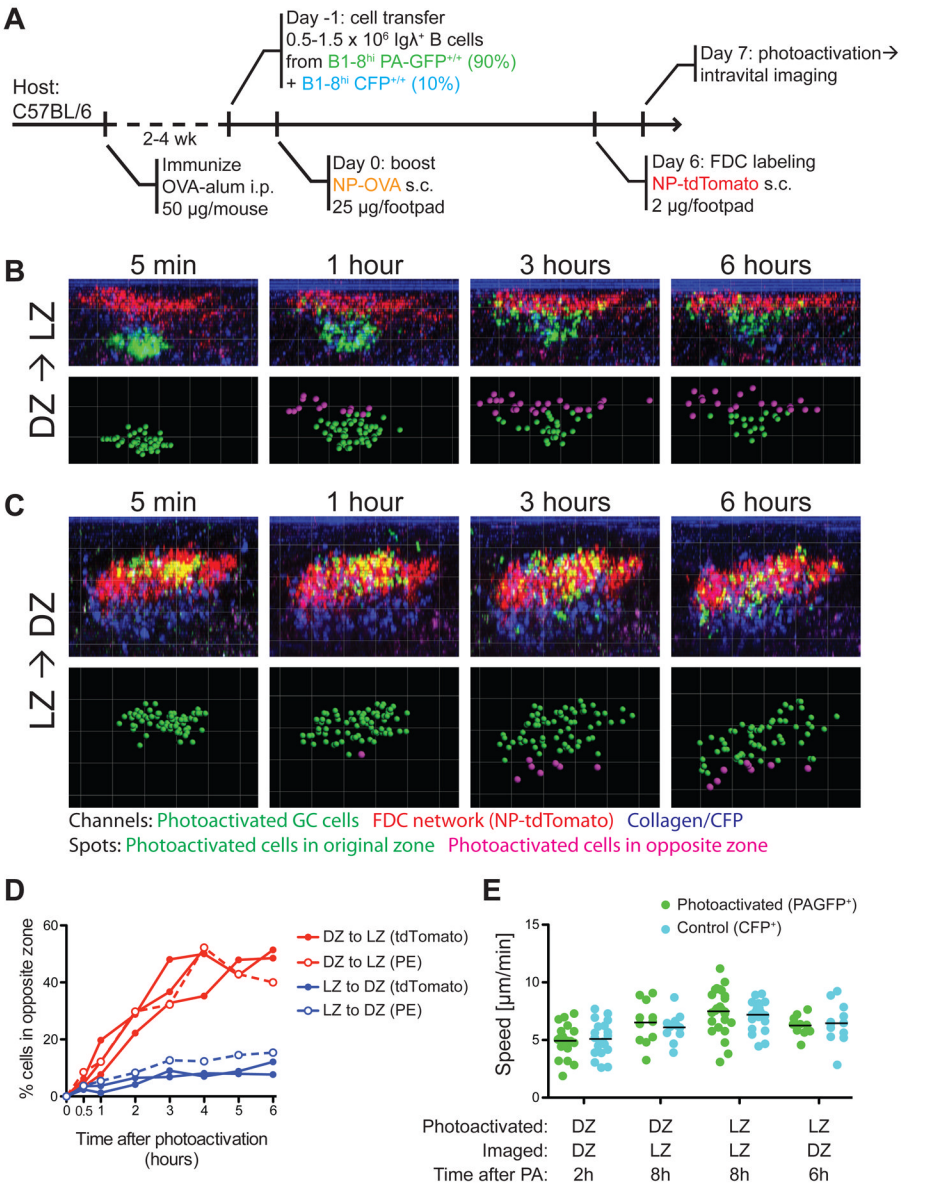

Figure 5. Interzonal migration in GCs

(A) Diagrammatic representation of the experimental protocol.

(B) Time series showing position of individual cells photoactivated in the DZ, at different times after photoactivation. Top row, side (X–Z) view of whole germinal centers within popliteal LNs of live mice. The LZ is labeled with NP-tdTomato (red); for better visualization, the PA-GFP signal shown (green) was isolated from autofluorescence and CFP bleed-through by co-localization filtering. Bottom row, spots were placed on photoactivated cells. Green spots indicate cells in the photoactivated zone, whereas magenta spots represent cells that have crossed over to the opposite (non-photoactivated) zone.

(C) Time series for cells photoactivated in LZ. Details as in (B).

(D) Quantification of seven independent experiments (three LZ to DZ and four DZ to LZ, one of which was terminated at 4 h). Closed symbols: LZ labeled by NP-tdTomato. Open symbols, LZ labeled by PE ICs.

(E) Speed of photoactivated GC cells and control CFP cells at different times after photoactivation. Each symbol represents one track; each column represents one cell type in one movie; bars represent the mean. Differences between $PAGFP^+$ and CFP^+ cells in the same movie were not significant ($p>0.5$) by Mann-Whitney U test. Different movies were acquired using different settings, and therefore should not be compared to each other.

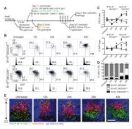

Figure 6. T cell help availability limits interzonal migration

(A) Diagrammatic representation of the experimental protocol.

(B) LZ/DZ distribution and DNA content (DAPI) analysis of DEC205$^{+/+}$ (top) and DEC205$^{-/-}$ (bottom) of popliteal lymph node GC B cells at different times after injection of αDEC-OVA.

(C) Quantification of (B). Each symbol represents one mouse.

(D) Fraction of GC cells derived from transferred DEC205$^{+/+}$ and DEC205$^{-/-}$ B1-8^{hi} and endogenous (DEC205$^{+/+}$) cells in popliteal lymph nodes of mice treated with αDEC-OVA for different lengths of time. Bar = standard error of mean.

(E) Histology showing the distribution of DEC205$^{+/+}$ cells in popliteal lymph node germinal centers at different times after injection of αDEC-OVA. DEC205$^{+/+}$ cells, which express PA-GFP (used here as a genetic label), were stained with anti-GFP antibodies (green). LZ and DZ can be identified by presence of CD35^{hi} follicular dendritic cells (FDCs, in red) and absence of IgD^{+} B cells (in blue), respectively.

All data representative of two experiments.

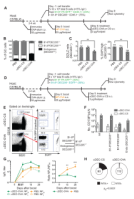

Figure 7. T cell help limits germinal center selection and affinity maturation

(A) Diagrammatic representation of the experimental protocol for panels B–D. PA-GFP is used as a genetic label in its non-activated form.

(B) Fraction of GC cells derived from transferred DEC205$^{+/+}$ and DEC205$^{-/-}$ B1-8^{hi} and endogenous (DEC205$^{+/+}$) cells in popliteal lymph nodes 72 hours after treatment with αDEC-OVA or αDEC-CS.

(C) DZ/LZ ratio and % cells in S/G2/M phase (DAPI high) among DEC205$^{+/+}$ and DEC205$^{-/-}$ popliteal lymph node GC B cells 72 hours after injection of αDEC-OVA or control αDEC-CS. ** $p < 0.01$, Kruskall-Wallis test, Dunn's post test.

(D) Diagrammatic representation of the experimental protocol for panels E and F. PA-GFP is used as a genetic label in its non-activated form.

(E) Plots show plasmablast/plasma cell gate (CD138^{hi}B220^{int}) and fraction of cells of each genotype, 72 hours after treatment with αDEC-OVA or αDEC-CS.

(F) Absolute number of CD138^{hi}/B220^{int} of each genotype per popliteal LN.

(A–F) Each symbol represents one mouse; data pooled from 2–3 experiments.

(G) Titers of total (NP_{23}) and high-affinity (NP_3) NP-reactive IgG1 (left) and total/high-affinity ratio (right) in NP-OVA-immunized wild-type mice treated or not with αDEC-OVA. Arrowheads indicate doses of treatment (details as in Fig. S6B). Pooled data from two experiments, five mice per group per experiment. Error bars represent SEM. ** $p < 0.01$, *** $p < 0.001$, Mann-Whitney U Test.

(H) Proportion of V186.2 clones bearing the high-affinity W33L mutation in day-14 wild-type germinal centers from mice treated with either αDEC-OVA or αDEC-CS (details as in Fig. S6C). The number of clones analyzed is indicated in the center of each chart. Pooled data from two experiments, three mice per experiment.